The 10th International Symposium on Flow Visualization
August 26-29, 2002, Kyoto, Japan
F0140

Visualization of Memory Effects on Multi-Scale Structures in Turbulence Near-Wake

Li, H.*[1], Zhou, Y.*[2], Takei, M.*[3], Saito, Y.*[4] and Horii, K.*[5]

*1 Department of Mechanical Engineering, Kagoshima University
1-21-40, Korimoto, Kagoshima 890-0065, Japan
Tel & Fax: +81-99-285-8252
E-mail: li@mech.kagoshima-u.ac.jp
*2 Department of Mechanical Engineering, The Hong Kong Polytechnic University, Hong Kong
*3 Department of Mechanical Engineering, Nihon University, Japan
*4 Department of Electrical & Electonic Engineering, Hosei University, Japan
*5 Shirayuri College, Japan

Abstract: The effects of initial conditions on turbulence structures of various scales in a near wake have been investigated for two wake generators with the same characteristic dimension, i.e. a circular cylinder and a screen of 50% solidity, based on the wavelet multi-resolution analysis. Measurements were made at x/h = 20. The wavelet multi-resolution technique was applied to decomposing the velocity data, obtained in the wakes generated by the two generators, into a number of wavelet components based on the central frequencies. The instantaneous sectional streamlines and vorticity field were thus 'visualized' for each wavelet component or central frequency. It was found that the behavior of large- and intermediate-scale structures depend on the initial conditions and the small-scale structures are independent of the initial conditions. The contributions from the wavelet components to the time-averaged Reynolds stresses and vorticity were estimated. Both the large-scale and intermediate longitudinal structures make the most significant contributions to Reynolds stresses in the circular cylinder wake, but the contribution from the large-scale structures appears dominating in the screen wake. The relatively small-scale structures of the circular cylinder wake contribute most to the total rms. spanwise vorticity.

Keywords: Orthogonal wavelet transform, Wavelet multi-resolution analysis, Initial condition, Turbulent structure, wake

1. Introduction

In the past decade, there has been a growing interest in the use of wavelet analysis for turbulent structures (Farge, 1992; Li, 1998). This technique can track turbulent structures in terms of time and scale, and extracts new information on turbulence structures of various scales. The continuous wavelet transform has been applied to analyzing turbulent structures in terms of time and scale by Li (1995 and 1998). This technique is capable of extracting continuously the characterization of local regularity, but it fails to reconstruct the original function from wavelet composition because of the non-orthogonal mother wavelet function. On the other hand, the discrete wavelet transform allows an orthogonal projection on a minimal number of independent modes and is invertible. Such

Copyright © 2002 by VSJ

analysis can produce a multi-resolution representation and might be also used to analyze turbulent structures of various scales. Charles (1991) first used the one-dimensional discrete wavelet transform to obtain local energy spectra and the flux of kinetic energy from experimental and direct numerical simulation data. Staszewski et al. (1997) identified the turbulent structures of the atmospheric boundary-layer using the discrete wavelet transform. Li et al. (2000 and 2001) employed discrete wavelet transforms to evaluate eddy structures of a jet in terms of time and scale. Li et al. (1999, 2001) also applied the two-dimensional orthogonal wavelets to turbulent images, and extracted the multi-resolution turbulent structures. Farge et al. (1999) developed a coherent vortex simulation method to decompose turbulent flows into coherent and incoherent structures based on orthogonal wavelets. To extract turbulent structures of various scales from the measured instantaneous multi-point velocity field, Li and Zhou (2000) proposed a new signal processing technique, i.e. vector wavelet multi-resolution analysis based on an orthogonal wavelet transform. Based on this technique, instantaneous turbulent structures of different scales can be separated and characterized.

It is now well established that the topology and transport characteristics of the turbulent structure in the wake depend on the wake-generating bodies or initial conditions (Screenivasan 1981; Wygnanski et al. 1986; Louchez et al. 1987; Matsumura et al. 1991; Zhou & Antonia 1995). A number of investigators have studied the effect of the initial conditions on the behavior of a near turbulent wake. Screenivasan (1981) found substantial differences in the manner wakes produced by different wake-generating bodies, even if the mean velocity profile exhibited the same shape. A dependence of the normalized distributions of the longitudinal turbulence intensity on the initial conditions was examined by Wygnanski et al. (1986). Although Louchez et al. (1987) and Matsumura et al. (1991) have confirmed that the vortical behavior in the wake differs as the initial conditions differ; this difference has not been well documented. Zhou and Antonia (1994a) studied turbulent near-wake vortices behind various wake-generating bodies and observed a significant variation in the flow structure and momentum transport characteristics of turbulent vortices with initial conditions. However, due to the limitation of their detection scheme, they could not provide any information on the dependence of organized structures other than the large-scale ones on the initial conditions. The question how the initial conditions produce an effect on the turbulent structure of various scales in a near turbulent wake is still open. It is suspected that the organized structures of various scales all contribute to the dependence of the turbulent topology and transport characteristics on the initial conditions.

The present work aims to study the effect of initial conditions on the turbulent structures of various scales. Measurements were conducted in the near-wake generated by a circular cylinder and a screen of 50% solidity, respectively. The wavelet multi-resolution analysis is used to decompose the measured velocity data into a number of wavelet components based on their central frequencies, which are representative of the turbulent structures of different scales. The flow structure of various scales is characterised and visualized by the sectional streamlines and vorticity contours of the decomposed wavelet components. The contributions the wavelet components make to the time-averaged Reynolds stress and the root mean square vorticity are estimated and compared between the two wake generators.

2. Wavelet Multi-resolution Analysis

2.1 Two-dimensional Orthogonal Vector Wavelet Transform

For a two-dimensional vector function $\vec{v}(x_1, x_2)$ and a wavelet basis $\Psi_{m;n_1,n_2}(x_1, x_2)$, the two-dimensional discrete vector wavelet transform is defined by

$$\overrightarrow{Dv}_{m;n_1,n_2} = \sum_i \sum_j \vec{v}(x_1^i, x_2^j) \Psi_{m;n_1,n_2}(x_1^i, x_2^j). \quad (1)$$

Here m is wavelet level, n_1 and n_2 the locations and $\overrightarrow{Dv}_{m;n1,n2}$ is called discrete vector wavelet transform coefficients. The two-dimensional orthogonal wavelet basis, $\Psi_{m;n_1,n_2}(x_1, x_2)$, is simply to

Copyright © 2002 by VSJ

take the tensor product functions generated by two one-dimensional orthogonal bases as

$$\Psi_{m;n_1,n_2}(x_1,x_2)=2^{-m}\psi\left(2^{-m}x_1-n_1\right)\psi\left(2^{-m}x_2-n_2\right). \tag{2}$$

In the basis the two variables x_1 and x_2 are dilated separately. The oldest example of a function $\psi(x)$ for which the $\psi_{m,n}(x)$ constitutes an orthogonal basis is the Haar function, constructed long before the term "wavelet" was coined. In the past ten years, various orthogonal wavelet bases have been constructed, for example, Meyer, Daubechies, Coifman, Battle-Lemarie, Baylkin, and spline. They provide good localization properties in physical and frequency spaces. Different wavelet bases will preferentially move, between scales, different characteristics of the target data sets. Examples like the use of Harr basis or low order wavelet basis may emphasize discontinuous in the target data sets since they have good localization property in physical space. However, the high order wavelet bases may emphasize the smoothness of the analyzed data and wavelet coefficients of each level contain more information in physical space, because they have good localization properties in frequency spaces.

Since the discrete vector wavelet transform is an orthogonal transform, it has the inverse transform and the original vector function can be reconstructed from the inversion of $\overrightarrow{Dv}_{m;n1,n2}$ as following:

$$\vec{v}(x_1,x_2)=\sum_{m}\sum_{n_1}\sum_{n_2}\overrightarrow{Dv}_{m;n_1,n_2}\Psi_{m;n_1,n_2}(x_1,x_2). \tag{3}$$

Like the Fourier transform, the discrete wavelet transform is linear operation that operates on the vector data whose length is an integer power of 2. The high level corresponds to small-scale or high-frequency. In general, the discrete vector wavelet transform can give a parsimonious representation of a vector function and can express the vector function in terms of a relatively small set of coefficients, which preserves the all features of the original vector function.

2.2 Vector Wavelet Multi-Resolution Analysis

As described in previous section, the discrete wavelet transform is an orthogonal and linear transform. Therefore, using Eq.(3) a non-linear vector function can be convert to an infinite summation of vector wavelet components at different central frequencies (from low frequency to high frequency), i.e.,

$$\vec{v}(x_1,x_2)=\overrightarrow{Mv}_1+\overrightarrow{Mv}_2+\cdots+\overrightarrow{Mv}_k, \tag{4}$$

where

$$\overrightarrow{Mv}_i=\sum_{n_1}\sum_{n_2}\overrightarrow{Df}_{i;n_1,n_2}\Psi_{i;n_1,n_2}(x_1,x_2) \tag{5}$$

This method is called the vector wavelet multi-resolution analysis. On the right side of Eq. (4), the first term $\overrightarrow{Mv}_1$ and the last $\overrightarrow{Mv}_k$ represent the wavelet components at level 1 (the lowest frequency) and level k (the highest frequency). It is evident that the vector wavelet multi-resolution analysis is an orthogonal decomposition processing.

The vector wavelet multi-resolution analysis can be summarized in two steps:

(1) Wavelet coefficients are computed based on the discrete wavelet transform of Eq. (1).

(2) Inverse wavelet transform of Eq. (3) is applied to wavelet coefficients at each wavelet level, and wavelet components are obtained at each level or scale.

It is evident that the sum of all frequency components is a reconstruction of the original vector function. Therefore, the wavelet multi-resolution analysis may process fewer data by selecting the relevant details that are essential to perform an extraction of the multi-scale flow structures, and decompose the vector data in both Fourier and physical spaces. In this study, the Daubechies family with index N=20 are used.

Copyright © 2002 by VSJ

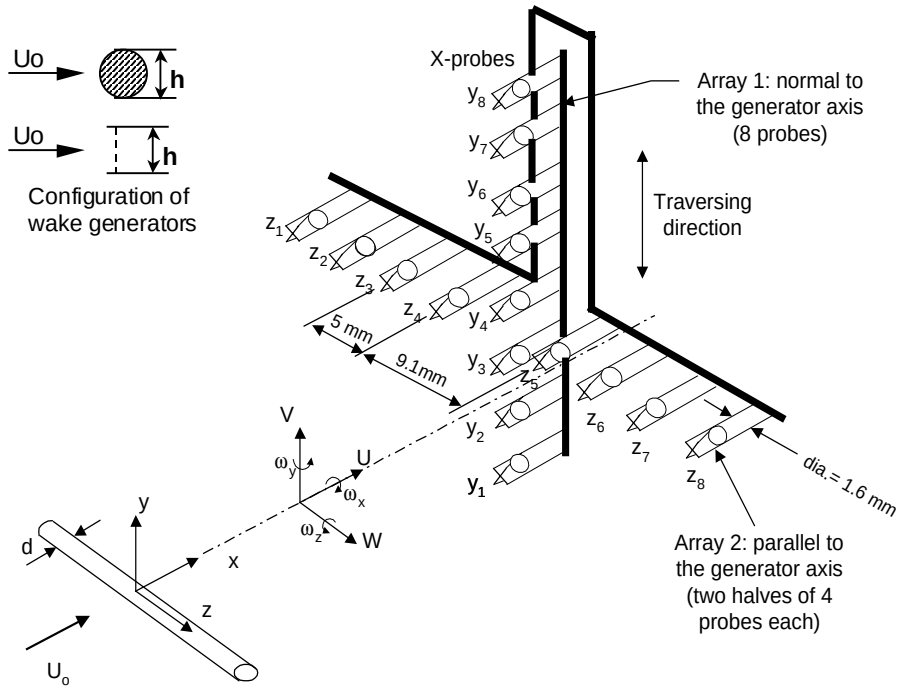

Fig.1 Experimental setup.

3. Experimental Setup

Experiments were conducted in an open-return low-turbulence wind tunnel with a 2.4 m-long working section (0.35 m x 0.35 m). The bottom wall was tilted to achieve a zero streamwise pressure gradient. Figure 1 shows the experimental arrangement. A circular cylinder and a screen of 50% solidity with the same height (h = 12.5 mm) were used to generate the wake, respectively; each was installed in the mid-plane and spanned the full width of the working section, 0.20 m from the exit plane of the contraction. This resulted in a blockage of about 3.6%. The stream-wise length of screen is about 0.5 mm. Measurements were made at x/h = 20 (x is the streamwise distance downstream of the cylinder) and a constant free stream velocity (U_0 = 6.7 m/s). The corresponding Reynolds number Re ($\equiv U_0 h/\nu$) was 5600.

Two orthogonal arrays, each consisting of eight X-wires, were used. One was aligned in the (x, y)-plane, i.e. the plane of mean shear, and the other in the (x, z)-plane, which was parallel to both the cylinder axis and the streamwise direction. The sixteen X-wires of the two arrays allow velocity fluctuations u and v in the (x, y)-plane and u and w in the (x, z)-plane to be obtained simultaneously. The nominal spacing between X-wires in both planes was about 5 mm except for a relatively large gap (= 9.1 mm) between the fourth and fifth X-wires in the (x, z)-plane. The arrays were attached to separate traversing mechanisms and could be moved independently of each other. The physical blockage caused by these arrays, cables and supports was estimated to be about 3%. Several types of measurements (Zhou & Antonia, 1994b) indicated that the interference to the flow due to the two arrays was negligible.

Wollaston (Pt-10% Rh) wires, 5 μm in diameter and about 1 mm in working length, were operated with constant temperature circuits. Signals from the circuits were offset, amplified and then digitized using two 16 channel (12bit) A/D boards and two personal computers at a sampling frequency of f_s = 3.5 kHz per channel (the cut-off frequency was 1600Hz). Data acquisition by the two computers was synchronized using a common external trigger pulse. The wires were calibrated for velocity and yaw, and continuously checked for drift. Using velocity and yaw calibrations, signals proportional to u, v and w, together with the local mean velocities $\overline{U}$, $\overline{V}$ (≈ 0) and $\overline{W}$ (≈ 0), were formed on a digital tape. The duration of each record was about 38 sec.

Copyright © 2002 by VSJ

4. Wavelet Decomposition Method of Turbulent Structures

An instantaneous velocity $U_i(x,y,z,t)$ can be written as the sum of a time-averaging component $\overline{U}_i(x,y,z)$ and a wavelet component $u_i(x,y,z,t)$, viz.

$$U_i(x,y,z,t)=\overline{U}_i(x,y,z)+u_i(x,y,z,t) \tag{11}$$

where the subscript *i* represents the wavelet component or wavelet level.

In order to gain insight into the turbulent structures of various scales, the wavelet multi-resolution technique is used to decompose the velocity fluctuation component $u_i(x,y,z,t)$ into a number of wavelet components based on wavelet levels, which correspond to the central frequencies and are directly linked to the turbulent structure scales. Each wavelet component represents the turbulent structures of a certain range of frequencies (i.e. a non-zero frequency band) so that the information of any scales contained in the original data will not be lost because of a limited number of wavelet levels. In the present study, thirteen wavelet levels are obtained, $u_i(x,y,z,t)$ being given by

$$u_i(x,y,z,t)=\sum_{j=1}^{13} u_{i,j}(x,y,z,t), \tag{12}$$

where $u_{i,j}(x,y,z,t)$ is the wavelet component of $u_i(x,y,z,t)$ at the *jth* wavelet level. Accordingly, the instantaneous velocity of the *jth* wavelet level is given by

$$U_{i,j}(x,y,z,t)=\overline{U}_i(x,y,z)+u_{i,j}(x,y,z,t). \tag{13}$$

The wavelet components of spanwise vorticity may be computed based on velocity data at each wavelet level using the central difference approximation. Thus, the eight X-wires in the (*x, y*)-plane may produce the thirteen wavelet components of spanwise vorticity at each of the seven midpoints between adjacent X-wires. The wavelet component of spanwise vorticity at the *jth* wavelet level may be approximated by

$$\omega_{zj}=\frac{\partial V_j}{\partial x}-\frac{\partial U_j}{\partial y}=\frac{\partial v_j}{\partial x}-\frac{\partial(\overline{U}+u_j)}{\partial y}\approx\frac{\Delta v_j}{\Delta x}-\frac{\Delta(\overline{U}+u_j)}{\Delta y}, \tag{14}$$

where $U_j=\overline{U}+u_j$ and $V_j\approx v_j$ ($\overline{V}\approx 0$). In Eq. (14), Δy (≈ 5.0 mm) is spacing between two X-wires in the (*x, y*)-plane; $\Delta x=-U_c\Delta t$. For simplicity, the average vortex convection velocity U_c = $0.87U_0$ on the vortex path (Zhou & Antonia 1992) is used to calculate Δx. Vorticity contours and rms values thus obtained showed no appreciable difference from those obtained using the local mean velocity.

5. Results and Discussion

The power spectrum (not shown) of the *v*-signal exhibits a prominent peak around the frequency f_0, which are 109 Hz and 145 Hz for the circular and screen wakes, respectively. Evidently, the frequency f_0 represents the average frequency of the large-scale vortical structures, i.e., Karman vortices.

5.1 Turbulent Structures of Various Scales

In order to 'visualize' instantaneous turbulent structures of various scales, sectional streamlines were constructed for each wavelet component of velocity as well as for measured velocities. Figure 2 shows the instantaneous sectional streamlines superimposed on the contours of normalized vorticity, $\omega_z h/U_0$, in the circular cylinder and screen wakes in the (*x, y*)-plane for the measured data. The same spatial scales have been used for the two flows to facilitate the comparison. The

Copyright © 2002 by VSJ

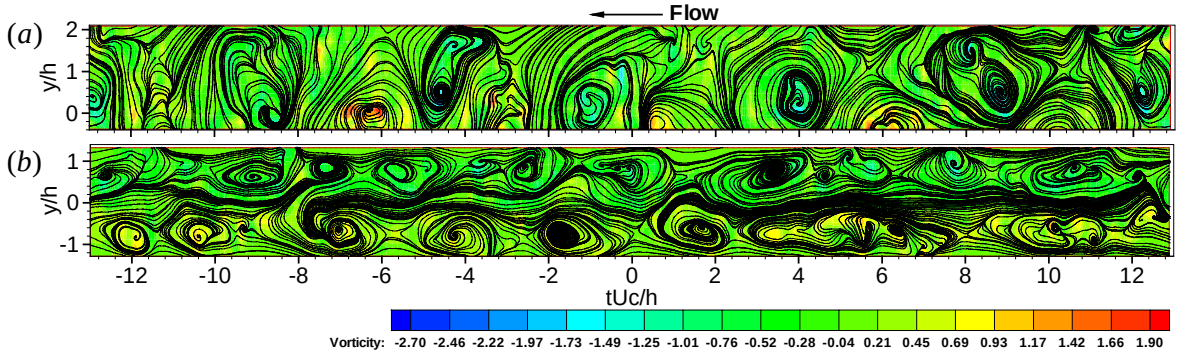

Fig.2 Measured sectional streamlines and vorticity contours, $\omega_z h/U_0$, in the (x, y)-plane. (a) cylinder; (b) screen.

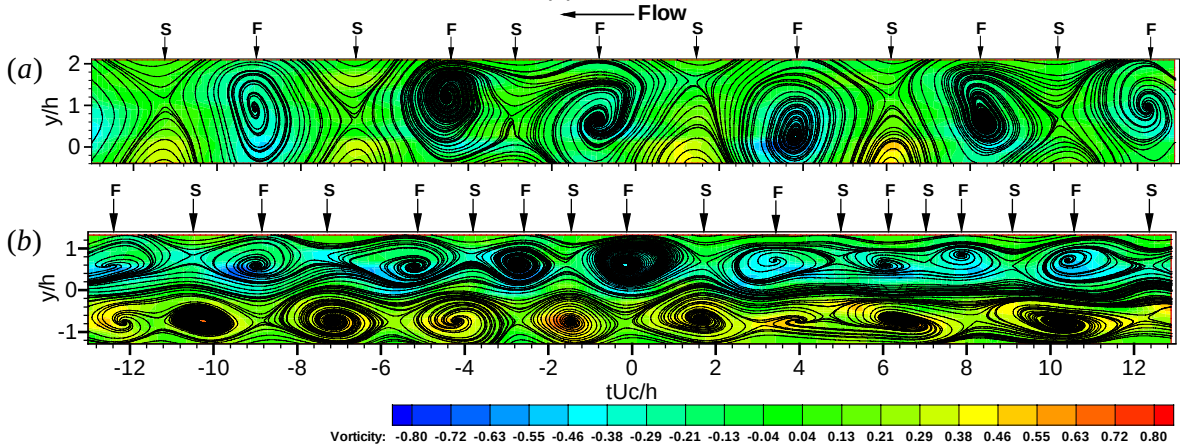

Fig.3 Sectional streamlines and vorticity contours, $(\omega_z)_{f_0} h/U_0$, of the wavelet component at f_0 in the (x, y)-plane. (a) cylinder; (b) screen.

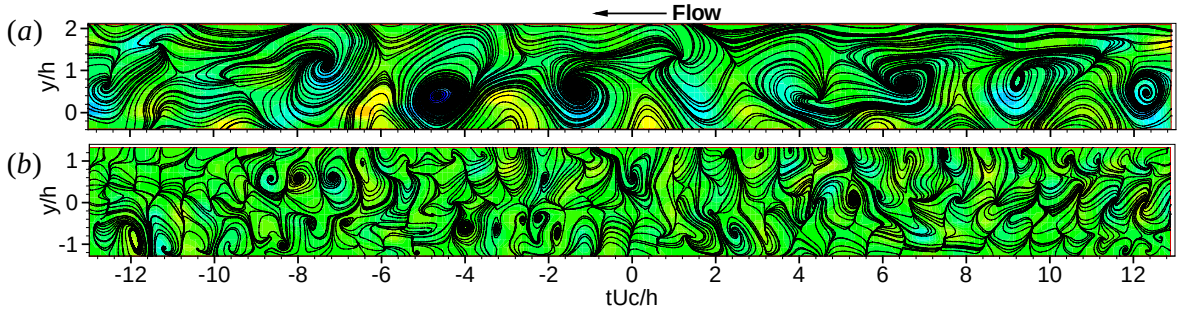

Fig.4 Sectional streamlines and vorticity contours, $(\omega_z)_{2f_0} h/U_0$, of the wavelet component at $2f_0$ in the (x, y)-plane. (a) cylinder; (b) screen. The color legend is as in Fig.3.

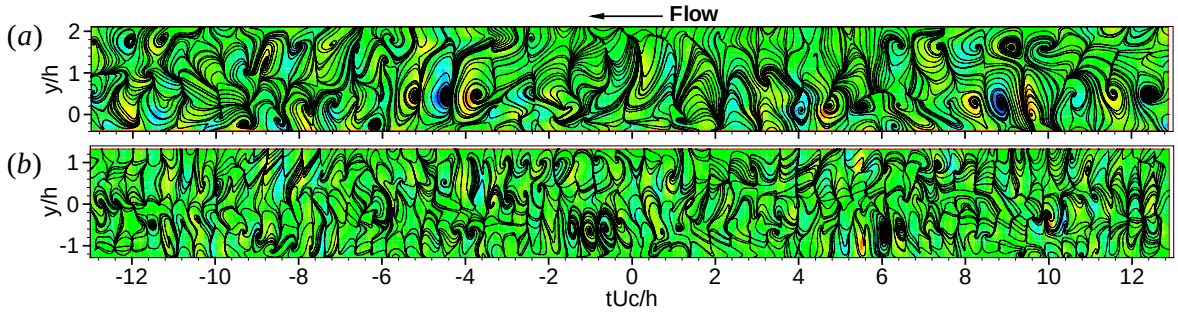

Fig.5 Sectional streamlines and vorticity contours, $(\omega_z)_{4f_0} h/U_0$, of the wavelet component at $4f_0$ in the (x, y)-plane: (a) cylinder; (b) screen. The color legend is as in Fig.3

Copyright © 2002 by VSJ

vertical axis is the spatial coordinate plotted in cylinder diameter units. The horizontal axis is the temporal coordinate plotted also in cylinder diameter units after converting the time displacements into spatial ones by using the average convection velocity of vortical structures. The timescale is increasing from left to right in such a way that the flow is observed moving from right to left. The false colors have been assigned to the scalar values of vorticity; the highest and lowest vorticities are respectively displayed as red and blue. The positive and negative vorticities denote clockwise and counterclockwise vortices, respectively. The vortical structures exhibit striking difference in geometrical shape, size, and spacing between the two wake generators. The maximum strength of spanwise vorticity in the circular cylinder wake is larger than that in the screen wake. However, only the large-scale structures are evident. It would be difficult to study the behaviours of the structures other than the large-scale ones for either flow.

Figures 3-5 present sectional streamlines and vorticity contours of different scales in the (x, y)-plane for the circular cylinder and screen wakes, calculated from the wavelet components of velocity at the central frequencies of f_0, $2f_0$ and $4f_0$. As discussed above, f_0 corresponds to the vortex shedding frequency of the circular cylinder and screen wakes. Perry and Chong (1987) proposed to use the theory of critical points to describe eddy motions and flow patterns. Zhou and Antonia (1994b) successfully applied this theory to studying the topological details and three-dimensional aspects of a turbulent wake. Critical points, in particular, foci and saddle points, represent the major topological characteristics of the flow. In general, the foci of the streamlines coincide with the local vorticity peaks, suggesting that information about the flow structure can be obtained by examining either streamlines or vorticity.

Figure 3(a) displays six vortical structures in the cylinder wake, corresponding quite well to the large-scale structures in Figure 2(a). The foci and saddle points, as denoted by F and S in Figure 3, respectively, coincide approximately with those in Figure 4 associated with large-scale structures. But the structures in Fig.3 appear better organized and exhibit a much stronger periodicity. The observation indicates a correspondence between the wavelet component of the central frequency f_0 and the large-scale Karman vorticies. Figure 3(b) exhibits nine pairs of vortices in the screen wake. These structures correspond quite well to the large-scale structures in Fig.2 (b), and their occurrence is rather periodical. They are apparently the uppermost and energy-containing structures. Again, we see a great difference in vortical structures between the two wakes. The structures in the circular cylinder wake are larger than those in the screen wake. Furthermore, the vortices in the screen wake are elliptical in shape. The maximum strength of spanwise vorticity in the circular cylinder wake, however, is smaller than that in the screen wake. These differences reflect basic differences in the vortex formation mechanisms. The vortices in the circular cylinder wake originate from the boundary layer separation from the cylinder. On the other hand, those in the screen wake are likely to arise from the shear layer instability in the developing wake. While the former, when advected downstream, are characterized by a decaying strength, the latter may have an increasing strength in the near wake (Zhang & Zhou 2001).

As the central frequency increases to $2f_0$ (Fig. 4), we see the structures of higher frequency but smaller size than those in Fig.3. Some of them are apparently associated with the large-scale vortices of f_0 (Figure 3), for example, at $tU_c/h \approx$ -1.2 and -4.6 in the circular cylinder wake and at $tU_c/h \approx$ -8 and -8.8 in the screen wake. Others correspond to the saddle region between the large-scale vortices, such as at $tU_c/h \approx$ -7.2 and 6.6 in the circular cylinder wake and at $tU_c/h \approx$ -6.4 and –7.0 in the screen wake. The latter structures are consistent with the occurrence of longitudinal or rib structures, which occur between successive spanwise structures (e.g. Hussain & Hayakawa 1987; Zhou & Antonia 1994b; Zhang et al. 2000). The size of the vortical structure and the maximum strength of spanwise vorticity in the circular cylinder wake appear larger than that in the screen wake.

Once the central frequency reaches $4f_0$ (Fig. 5), the structures of smaller scale appear all over the flow. The structures in the circular cylinder wake appear considerably larger than those in the screen wake. The structures appear to have positive and negative vorticity concentrations aligned periodically along the flow direction. This periodicity appears to be stronger in the screen wake than in the cylinder wake.

Copyright © 2002 by VSJ

5.2 Contributions to the Reynolds Stresses and Vorticity Variance from Different Wavelet Components

The wavelet components of the time-averaged Reynolds stress and root mean square (rms.) vorticity, $\overline{u_j^2}$, $\overline{v_j^2}$, $\overline{u_j v_j}$ and $\overline{\omega_j^2}$, represent the contributions from the turbulent motions of various scales to the Reynolds stresses and vorticity. They are calculated from the wavelet components of instantaneous velocity and vorticity and compared between different central frequencies.

5.2.1 Reynolds Stresses

Figure 6 presents the lateral distributions of $\overline{u_j^2}$, $\overline{v_j^2}$ and $\overline{u_j v_j}$, as compared with the measured values for the circular cylinder and screen wakes. The results are normalized by the maximum value of the measured $(\overline{fg})_{\max}$, where f or g each represents u or v, so as to indicate the contribution from each wavelet level or central frequency to the Reynolds stresses. The negative $\overline{u_j v_j}/(\overline{uv})_{\max}$ near y/h = 0 and at relatively high central frequencies has been removed in Fig.6 (c) to allow the log-scale presentation. The $(\overline{fg})_{\max}$ values show discernible difference between the circular-cylinder and the screen wakes, in particular for $(\overline{u^2})_{\max}$ and $(\overline{v^2})_{\max}$. The observation is in consistence with the results of Zhou & Antonia (1994a), suggesting the effect of different generators. The wavelet component of the central frequency f_0 represents the large-scale vortical structures. The distributions of $\overline{f_j g_j}/(\overline{fg})_{\max}$ are similar to that of the measured data for both circular cylinder and screen, varying greatly with the central frequency. For y/h > 1.2, $\overline{f_j g_j}/(\overline{fg})_{\max}$ of the screen wake is smaller than that of the circular cylinder wake and tends to fall off quickly, approaching zero. The $\overline{f_j g_j}/(\overline{fg})_{\max}$ value of f_0 in the screen wake is larger than that in the circular cylinder wake for y/h < 1.0 (not so evident in Fig.6 because of the use of log scale). The observation suggests that the coherent contribution from the large-scale vortical structures to the Reynolds stresses is larger in the porous body near-wake than in the solid body near-wake. The result again confirms the conception that the large-scale vortical structures contribute to the effect of initial conditions on the near wake. Furthermore, the difference between the two wakes is appreciable down to the wavelet components of $4f_0$, suggesting that the intermediate-scale structures also play a role in the

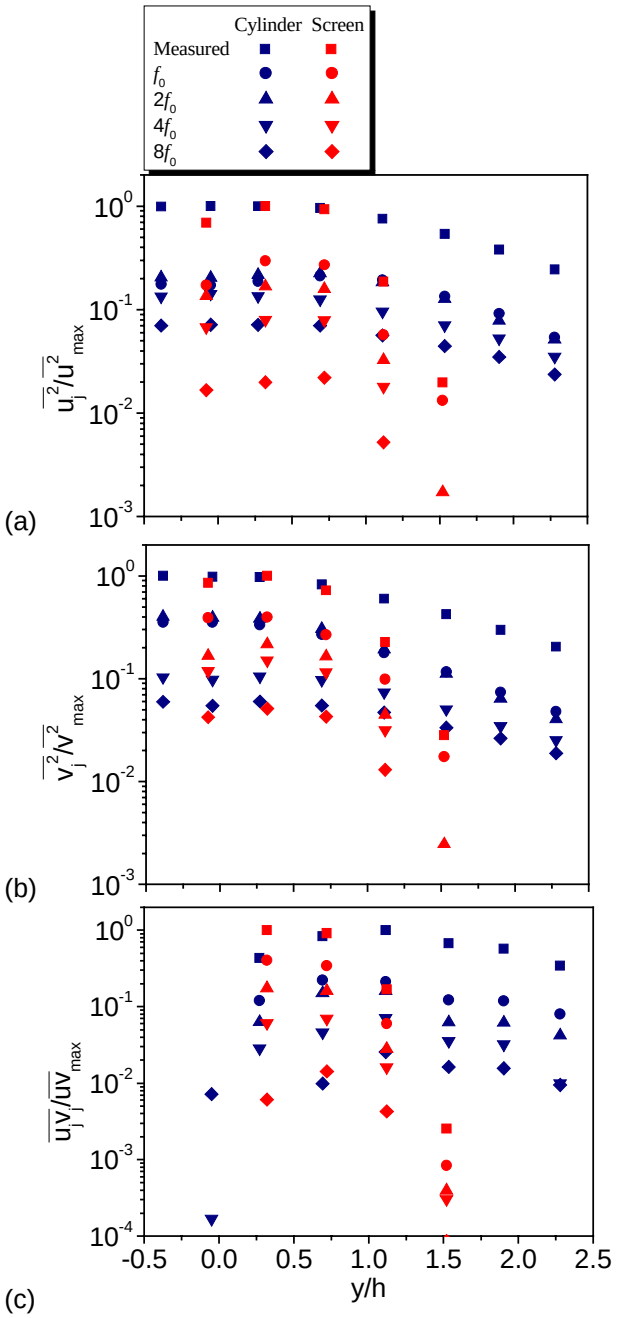

Fig. 6 Velocity variance of the measured and the wavelet components at various central frequencies

Copyright © 2002 by VSJ

persistence of the initial conditions. In general, the value of $\overline{f_j g_j}/(\overline{fg})_{max}$ decreases as the central frequency increases, being consistent with the perception that the lower frequency eddies are energy-containing. For the central frequency greater than $4f_0$, $\overline{f_j g_j}/(\overline{fg})_{max}$ tends to fall off quickly, approaching zero.

In the case of the circular cylinder wakes, $\overline{u_j^2}/(\overline{u^2})_{max}$ and $\overline{v_j^2}/(\overline{v^2})_{max}$ of $2f_0$ are very close to that of f_0, implying that energies associated with the two central frequencies are quite comparable. As a matter of fact, the former even exceeds, though slightly, the latter near the centreline. This is because the lateral spacing between the two rows of vortices is small in the near-wake and thus the most prominent peak in the fluctuating velocity spectra (not shown) occurs at the second harmonic of the vortex shedding frequency near the centreline. Furthermore, the wavelet components at f_0 and $2f_0$ are most energy-containing; they account for almost 43%, 74% and 40% of $(\overline{u^2})_{max}$, $(\overline{v^2})_{max}$ and $(\overline{uv})_{max}$, respectively. This indicates a significant contribution from the intermediate-scale structures to the total Reynolds stresses. The value of the wavelet component appears falling off rather rapidly, up to about 11% of the measured value for $\overline{v_j^2}/(\overline{v^2})_{max}$ when the central frequency increases from $2f_0$ to $4f_0$.

For the screen wake, $\overline{f_j g_j}/(\overline{fg})_{max}$ of f_0 remains everywhere largest value and accounts for almost 40%, 29% and 40% of $(\overline{u^2})_{max}$, $(\overline{v^2})_{max}$ and $(\overline{uv})_{max}$, respectively. The decrease is rather rapid, up to 17~22% of the measured $(\overline{fg})_{max}$, when the central frequency increases from f_0 to $2f_0$. This indicates that the greatest contribution to the total Reynolds stresses comes from the large-scale structure in the screen wake.

The above observation indicates that the most significant contribution to the Reynolds stresses comes from the turbulence structures of f_0 and $2f_0$ in the cylinder wake. However, in the screen wake, the contribution to Reynolds stresses comes primarily from the turbulence structures of f_0; the role played by those of $2f_0$ appears to be less significant than that in the cylinder wake. This is a significant difference between the two wakes.

It is pertinent to comment that $\overline{v_j^2}/(\overline{v^2})_{max}$ (74%) corresponding to f_0 and $2f_0$ overwhelms $\overline{u_j^2}/(\overline{u^2})_{max}$ (43%) in the cylinder wake, which is similar to the behaviour of the coherent contribution from the large-scale structures in solid bluff-body wakes (Zhou & Antonia 1994b). In contrast, $\overline{u_j^2}/(\overline{u^2})_{max}$ (40%) at f_0 exceeds $\overline{v_j^2}/(\overline{v^2})_{max}$ (29%) in the screen wake, resembling the behaviour of the coherent contribution from the large-scale structures in a turbulent far-wake (Zhou & Antonia 1994b). The different behaviour between the large-scale structures in the two wakes corroborates the proposition that their vortex generation mechanisms are not the same.

5.2.2 Vorticity Variance

Figure 7 presents the spanwise measured vorticity variance, $\overline{\omega_z^2}/(\overline{\omega_z^2})_{max}$, and the wavelet components, $\overline{\omega_{zj}^2}/(\overline{\omega_z^2})_{max}$, where $(\overline{\omega_z^2})_{max}$ is the maximum value of the measured vorticity. The variation of $\overline{\omega_{zj}^2}/(\overline{\omega_z^2})_{max}$ with y/h is qualitatively similar

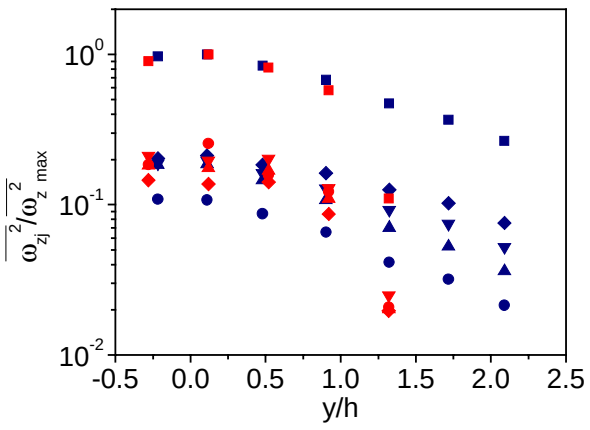

Fig. 7 Spanwise vorticity variance of the measured and the wavelet components at various central frequencies. The symbols are as in Fig.6

Copyright © 2002 by VSJ

to $\overline{\omega_z^2}/(\overline{\omega_z^2})_{\max}$. Both $\overline{\omega_z^2}/(\overline{\omega_z^2})_{\max}$ and $\overline{\omega_{zj}^2}/(\overline{\omega_z^2})_{\max}$ drop towards the free-stream. The drop is particularly fast for the screen wake. Interestingly, $\overline{\omega_{zj}^2}/(\overline{\omega_z^2})_{\max}$ of the circular cylinder corresponding to f_0 is now smallest, accounting for about 11% of the total vorticity variance. This indicates a relatively small contribution to the total vorticity variance from the large-scale structures. This contribution increases considerably at $2f_0$, up to about 19%, and continues to rise as the central frequency increases, reaching the maximum, about 21%, at $8f_0$. Evidently, the intermediate- and relatively small-scale structures make a major contribution to the total vorticity variance. In contrast to the cylinder wake, the difference in $\overline{\omega_{zj}^2}/(\overline{\omega_z^2})_{\max}$ between different central frequencies is smaller for the screen wake. The value of $\overline{\omega_{zj}^2}/(\overline{\omega_z^2})_{\max}$ at f_0 even reaches largest near the centerline, accounting for about 25%, though giving way to the component at $4f_0$ for $y/h \gtrsim 0.5$. This could be because vorticity is generated under the effect of the shear layer instability in the wake, irrespective of its scales. On the other hand, in the cylinder wake, the vorticity of larger scales, typically at f_0, originates from the boundary layer separation from the cylinder, while the vorticity of other scales could be due to the interactions between the large-scale structures or the effect of the shear layer instability in the wake, as in the screen wake. The observation again reflects the basic difference in the vortex formation mechanisms between the circular cylinder and screen wakes.

6. Conclusions

The following conclusions can be drawn.

(1) The vortical structures at the central frequency of f_0 are consistent with the conditionally averaged large-scale structures for both wake generators (Zhou & Antonia 1994b). These structures, along with those of intermediate-scales exhibit a strong dependence upon the initial conditions. However, the small-scale structures at a central frequency more than $8f_0$ are less independent of the initial conditions.

(2) The contributions to the Reynolds stresses are comparable from the turbulent structures of f_0 and $2f_0$ in the circular cylinder wake, their combined contribution accounting for 43%, 74% and 40% to $(\overline{uv})_{\max}$, $(\overline{u^2})_{\max}$ and $(\overline{v^2})_{\max}$, respectively. In the screen wake, however, the structures of f_0 make a contribution considerably higher than other wavelet components, responsible for almost 40%, 29% and 40% to $(\overline{uv})_{\max}$, $(\overline{u^2})_{\max}$ and $(\overline{v^2})_{\max}$, respectively.

(3) For the circular cylinder wake, the relatively small-scale structures of $8f_0$ contribute most, about 21%, to the spanwise vorticity variance. On the other hand, the large-scale structures contribute only 11% to $(\overline{\omega_z^2})_{\max}$. This is different in the screen wake. The contribution to the vorticity variance from the structures of f_0 is quite comparable to that of other components. The above observations are consistent with the fact that the generation mechanism of the large-scale structures is different for the two wakes. While the large-scale structures in the circular cylinder wake are generated from the boundary layer separation from the cylinder, those in the screen wake may originate from the shear layer instability in the wake.

Acknowledgement

First author wishes to acknowledge support given to him by Grant-in-Aid for Scientific Research (C) (No.13650189) from Japanese Society for the Promotion of Science.

References

Charles, M., “Analysis of Turbulence in the Orthonormal Wavelet Representation”, Journal of Fluid Mechanics, Vol.232 (1991), pp.469-520.

Farge, M., “Wavelet Transforms and Their Applications to Turbulence”, Annu. Rev. Fluid Mech. Vol.24 (1992), pp.395-457.

Copyright © 2002 by VSJ

Farge, M., Schneider, K. and Kevlahan, N., “Non-Gaussianity and Coherent Vortex Simulation For Two-Dimensional Turbulence Using An Adaptive Orthogonal Wavelet Basis”, Physics of Fluids, Vol.11 (1999), pp.2187-2201.

Hussain, A.K.M.F. and Hayakawa, M. “Eduction of large-scale organised structures in a turbulent plane wake,” J. Fluid Mech. Vol.180 (1987), 193.

Li, H., “Identification of Coherent Structure in Turbulent Shear Flow with Wavelet Correlation Analysis”, ASME Journal of Fluids Engineering, Vol. 120 (1998), pp.778-785.

Li, H. and Nozaki, T., “Wavelet Analysis for the Plane Turbulent Jet (Analysis of Large Eddy Structure)”, JSME International Journal, Fluids and Thermal Engineering, Vol.38 (1995), pp.525-531.

Li, H., Takei, M., Ochi, M., Saito, Y., and Horii, K, “Application of Two-dimensional Orthogonal Wavelets to Multi-resolution Image Analysis of a Turbulent Jet”, Transactions of the Japan Society for Aeronautical and Space Sciences, Vol. 42 (1999), pp.120-127.

Li, H., Takei, M., Ochi, M., Saito, Y. and Horii, K., “Eduction of Unsteady Structure in a Turbulent Jet by using of Continuous and Discrete Wavelet Transforms”, Transactions of the Japan Society for Aeronautical and Space Sciences, Vol.42 (2000), pp.39-44.

Li, H., Takei, M., Ochi, M., Saito, Y. and Horii, K., “Wavelet Multiresolution Analysis Applied to Coherent Structure Eduction of a Turbulent Jet”, Transactions of the Japan Society for Aeronautical and Space Sciences, Vol.42 (2001), pp.203-207.

Li, H., Hu, H., Kobayashi, T., Saga, T. and Taniguchi, N., “Visualization of Multi-scale Turbulent Structure in Lobed Mixing Jet Using Wavelets”, Journal of Visualization, Vol.4 (2001), No.3, pp.231-238.

Louchez, P.R., Kawall, J. G. and Keffer, J. F., “Detailed Spread on Characteristics of Plane Turbulent Wakes”, Lecture Notes in Physics, Springer-Verlag, Berlin (1987), pp.98-109.

Matsumura, M., Huang, Z., Kawall, J. G. and Keffer, J. F., “Coherent Structures in the Turbulent Wake of a Porous Body”, Proceedings of the Eighth Symposium on Turbulent Shear Flows (1991), pp.28-2-1-28-2-6.

Perry, A.E. and Chong, M.S., “A Description of Eddy Motions and Flow Patterns Using Critical-Point Concepts”, Ann. Rev. Fluid Mech., Vol.19 (1987), pp.125-155.

Sreenivasan, K. R., “Approach to Self-Preservation in Plane Turbulent Wakes”, AIAA Journal, Vol.19 (1981), pp.1365-1367.

Staszewski, W. J., Worden, K. and Rees, J. M., “Analysis of Wind Fluctuations Using the Orthogonal Wavelet Transform”, Applied Scientific Research, Vol.59 (1997), pp.205-218.

Zhang, H.J. & Zhou, Y. “Effect of Unequal Cylinder Spacing on Vortex Streets behind Three Side-by-Side Cylinders”. Physics of Fluids, Vol.13 (2001), pp.3675-3686.

Zhang H.J., Zhou, Y. and Antonia, R.A. “Longitudinal and spanwise structures in a turbulent wake”, Physics of Fluids, Vol.12 (2000), pp.2954-2964.

Zhou, Y. and Antonia, R.A., “Convection Velocity Measurements in a Cylinder Wake”, Experiments in Fluids, Vol. 13 (1992), pp.63-70.

Zhou, Y. and Antonia, R.A., “Effect of Initial Conditions on Vortices in a Turbulent Near Wake”, AIAA Journal, Vol. 32 (1994a), pp.1207-1213.

Zhou Y. and Antonia R.A., “Critical points in a turbulent near-wake”, Journal of Fluid Mechanics, Vol.275 (1994b), pp.59-81.

Zhou, Y. and Antonia, R.A., “Memory Effects in Turbulent Plane Wakes”, Experiments in Fluids, Vol.19 (1995), pp.112-120.

Wygnanski, I., Champagne, F. and Marasli, B., “On the Large-scale Structures in Two-dimensional, Small-deficit, Turbulent Wakes”, Journal of Fluid Mechanics, Vol. 168 (1986), pp.31-71.

Copyright © 2002 by VSJ